Journal of Molecular Catalysis A: Chemical 403 (2015) 77–83

Contents lists available at ScienceDirect

Journal of Molecular Catalysis A: Chemical

journal homepage: www.elsevier.com/locate/molcata

Metal halides supported on mesoporous carbon nitride as efficient heterogeneous catalysts for the cycloaddition of CO_2

Jie Xu*, Fei Wu, Quan Jiang, Jie-Kun Shang, Yong-Xin Li*

Jiangsu Key Laboratory of Advanced Catalytic Materials and Technology, School of Petrochemical Engineering, Changzhou University, Gehu Road 1, Changzhou, Jiangsu 213164, PR China

ARTICLE INFO

Article history:
Received 3 February 2015
Received in revised form 30 March 2015
Accepted 30 March 2015
Available online 2 April 2015

Keywords:
Carbon nitride
CO_2 conversion
Cycloaddition
Propylene carbonate (PC)

ABSTRACT

A series of $ZnCl_2$/mp-C_3N_4 catalysts were prepared through a wet impregnation method using mesoporous g-C_3N_4 materials as catalytic supports. The physicochemical properties of the $ZnCl_2$/mp-C_3N_4 catalysts were characterized using several techniques, including N_2 adsorption–desorption, X-ray diffraction, Fourier transform infrared, UV–vis diffuse reflectance, and X-ray photoelectron spectroscopy. In the cycloaddition reactions of CO_2 with propylene oxide (PO) to propylene carbonate (PC), the $ZnCl_2$/mp-C_3N_4 materials revealed high catalytic performances at 140 °C and 6 h. Furthermore, other metal halides including $ZnBr_2$, $CoCl_2$, $FeCl_3$, $NiCl_2$, and $MgCl_2$ catalysts supported on mp-C_3N_4 were fabricated and the synthesized catalysts also demonstrated high performances in the catalytic cycloaddition of CO_2. A possible catalytic mechanism has been proposed. The mp-C_3N_4 material served mainly as a basic support to adsorb CO_2 whereas the supported metal halides were active sites to promote the activation of PO and realize its transform into PC.

1. Introduction

Notwithstanding being a major greenhouse gas, carbon dioxide (CO_2) is an abundant, nontoxic, economic, and renewable C1 building block [1,2]. Within the past decades, concerns about anthropogenic emissions along with climate change have sparked global interest in the chemical transformation of CO_2 to valuable chemicals [3,4]. One of the most interesting protocols utilizing CO_2 as a raw material is the cycloaddition of CO_2 with epoxides (e.g. propylene oxide, PO) to cyclic carbonates (e.g. propylene carbonate, PC) [5,6]. Such products are among the most important feedstocks which are extensively used as aprotic polar solvents, electrolyte components in lithium batteries, precursors for polycarbonates, and intermediates in organic synthesis [7,8].

A wide range of catalysts, both homogeneous and heterogeneous systems, have been developed for the cycloaddition of CO_2 to cyclic carbonates. Among them, ionic liquids (ILs) [9], organometallic complexes [2], quaternary ammonium [7] and phosphonium [1,10] salts have been proved to be the most efficient catalysts [3,11]. Despite the excellent catalytic activities, due to their intrinsic homogeneous nature, the main drawback in the use of such catalysts is the difficulty in catalyst recovery and product purification. By contrary, heterogeneous catalysts, including grafted ILs [12–14], modified molecular sieves [8], smectites [15,16], and mixed metal oxides [17,18], etc, offer technical advantages in the catalyst–product separation and reactor design [18]. However, the solid catalysts still suffer from low catalytic activity and/or selectivity. In this context, it is of high interest to explore and develop a novel catalyst which can afford high catalytic activity as well as convenient catalyst separation [6].

Recently, owing to its unique combination of multiple physicochemical properties, graphitic carbon nitride (g-C_3N_4) has attracted a great deal of attention and also been proposed as the most promising candidate to complement traditional carbon materials [19]. Up to now, g-C_3N_4, especially mesoporous g-C_3N_4 having large surface areas and rich pores, has been widely applied in numerous research fields, including photocatalysis [20,21], fuel cells [22,23], gas storage [24], and heterogeneous catalysis [25–28]. As an analogue to graphite, g-C_3N_4 possesses two-dimensional stacked structures with π-conjugated planar layers. In particular, at the edges of the graphitic sheets, there exist a large number of uncondensed terminal amine and imine groups [26,29]. The characteristic structures thus enable g-C_3N_4 as a typical solid base material. Ansari et al. [30,31] synthesized a series of mesoporous g-C_3N_4 materials using nanocasting approaches, and found the synthesized g-C_3N_4 could catalyze various CO_2-invloving transformations. Likewise, Huang et al. [32] prepared g-C_3N_4/SBA-15 via a chemical vapor deposition method and investigated the catalytic performance in cycloaddi-

* Corresponding authors. Tel.: +86 519 86 330 135.
E-mail addresses: shine6832@163.com (J. Xu), liyxluck@163.com (Y.-X. Li).

http://dx.doi.org/10.1016/j.molcata.2015.03.024
1381-1169/

tion of CO_2 to cyclic carbonates. Despite the above pioneer work, it should be noted that the basic sites of g-C_3N_4 (or even mesoporous g-C_3N_4) belong to weak base [33,34]. Hence, in the base-centered CO_2-activiating reactions, the catalytic activity was limited, and thus rigorous reactions conditions were demanded.

Zinc halides (e.g. $ZnCl_2$) are also high-performance catalysts for the cycloaddition of CO_2 with epoxide as it has been revealed that Zn^{2+} cations could activate the epoxide molecule by the coordination of oxygen atom thereof [1,3]. On the other hand, Zhu et al. [35] reported that Zn-doped g-C_3N_4 sample demonstrated superior activity to the bare g-C_3N_4 in the NO decomposition. Inspired by the reports, in the present contribution, we prepared mesoporous-g-C_3N_4-supported $ZnCl_2$ catalysts via a simple wet impregnation method. In the cycloaddition reactions of CO_2 with PO to PC, the $ZnCl_2$/mp-C_3N_4 catalysts demonstrated high activity, affording a maximum a PO conversion of 73%. Moreover, it has been also found that other metal halides catalysts supported on mp-C_3N_4 could catalyze the reactions with high performance.

2. Experiment

2.1. Preparation of mp-C_3N_4

The mesoporous C_3N_4 was prepared according to an established nanocasting method reported previously [25]. 4 g of cyanamide was dissolved in 16 g of aqueous suspensions of 12 nm silica spheres (Ludox HS40, Aldrich) under vigorous stirring. The mixture was heated in an oil bath at 50 °C under stirring overnight to remove water. The resultant white solid was ground in a mortar, transferred into a covered crucible, and heated at 3 °C min^{-1} up to 550 °C and then treated for further 4 h. Afterwards, the as-synthesized yellow powder was ground and immersed into 200 mL of NH_4HF_2 aqueous solution (4 mol L^{-1}) for 2 days to remove the template. Then, the dispersion was centrifuged and the yellow precipitate was washed using distilled water and ethanol for several times. Finally, the yellow sample was dried at 50 °C under vacuum overnight and the mass of the obtained C_3N_4 was *ca.* 1.8 g. The resulting C_3N_4 sample was designated as mp-C_3N_4.

2.2. Preparation of $ZnCl_2$/mp-C_3N_4

0.1 g of $ZnCl_2$ (0.73 mmol) was dissolved into 20 mL of absolute ethanol. 1 g mp-C_3N_4 was then added into the solution and stirred for 1 h. Next, the mixture was heated in a bath at 50 °C for several hours to remove ethanol. The obtained yellow solid was calcinated at 300 °C for 2 h under N_2 atmosphere. The resultant material was labeled as *m*$ZnCl_2$/mp-C_3N_4, where *m* indicated the loading amount (wt%).

2.3. Sample characterization

X-ray diffraction patterns were recorded with a Rigaku D/max 2500 PC X-ray diffractometer equipped with a graphite monochromator (40 kV, 40 mA) using Ni-filtered Cu-*Kα* radiation (λ = 1.5418 Å).

Nitrogen adsorption–desorption isotherms were measured at −196 °C using a Micromeritics ASAP 2020 analyzer. Prior to the analysis, the samples were degassed (10 μmHg) at 150 °C for at least 4 h. The specific surface area was calculated according to the Brunauer–Emmet–Teller (BET) method, and pore size distribution was determined by the Barret–Joyner–Halenda method.

Transmission electron microscopy (TEM) experiments were conducted on a JEOL 2010 electron microscope operating at 200 kV. Before being transferred into the TEM chamber, the samples dispersed in ethanol were deposited onto holey carbon films supported on Cu grids.

UV–vis diffuse reflectance spectra (DRS) were recorded on a Shimizu UV-3600 spectrophotometer. $BaSO_4$ was used as a standard reference. Each sample was pressed into a thin tablet and tested under ambient conditions. The absorption spectrum was calculated from the reflectance data with Kubelka–Munk function.

Fourier transform infrared (FT-IR) spectra of the samples were collected in transmission mode from KBr pellets at room temperature on a Bruker Tensor 27 spectrometer with a resolution of 4 cm^{-1}, using 32 scans per spectrum in the region of 400–4000 cm^{-1}. The mass ratio of every sample to KBr was constant at 1:100.

X-ray photoelectron spectroscopy (XPS) measurements were performed using a Perkin–Elmer PHI 5000C spectrometer working in the constant analyzer energy mode with Mg *Kα* radiation as the excitation source. The carbonaceous C 1s line (284.6 eV) was used as the reference to calibrate the binding energies.

2.4. Catalytic test

The cycloaddition of CO_2 with PO was carried out in 80 mL stainless steel autoclave equipped with a magnetic stirrer. In a typical reaction process, 7 mL of PO, 3 mL *N*,*N*-dimethyl formamide (DMF), and 0.2 g of the catalyst were added into the reactor. Then, the reactor was pressurized with CO_2 to a desired pressure and heated to 140 °C under stirring for 6 h. After the reaction, the autoclave was cooled down to the room temperature in ice water and the excess of CO_2 was vented. The liquid product was separated by centrifugation and analyzed using a GC equipped with a SE-54 capillary column and FID. The liquid mixture consisted of DMF, PO, PC, and 1,2-propylene glycol (PG) as the byproduct originating from the hydrolysis of PO with trace H_2O. No other substance was detected. The carbon balance was nearly 100%. Their quantitative calculation (i.e. conversion of PO, and selectivity to PC) was based on an area-normalization method.

The PO conversion and selectivity to PC were calculated as follows:

$$\text{Conv.} = \frac{A_{PC} \times f_{PC} + A_{PG} \times f_{PG}}{A_{PO} + A_{PC} \times f_{PC} + A_{PG} \times f_{PG}},\ \text{Sel.} = \frac{A_{PC} \times f_{PC}}{A_{PC} \times f_{PC} + A_{PG} \times f_{PG}} \quad (1)$$

where *A*, and *f* were the peak area of GC, and response factor for each product.

3. Results and discussions

3.1. Structure characterization

Fig. 1 displays the XRD patterns of mp-C_3N_4 and $ZnCl_2$/mp-C_3N_4 materials with various loading amounts. The XRD pattern of mp-C_3N_4 revealed a pronounced peak at $2\theta = 27.6°$ ($d = 0.323$ nm), indexed as (0 0 2) planes, which was characteristic stacking of the conjugated aromatic system [25,36]. In addition, a minor peak with low intensity was also observed at $2\theta = 13.2°$, which was attributed to the in-plane structural packing motif, e.g. the hole-to-hole array of nitride pores [37]. Likewise, whereas the whole intensity of the diffraction peaks decreased upon introducing $ZnCl_2$, the $ZnCl_2$/mp-C_3N_4 demonstrated similar XRD patterns to the pure mp-C_3N_4 sample, suggesting that the overall graphitic structures of mp-C_3N_4 have undergone no significant variation.

N_2 adsorption–desorption isotherms of mp-C_3N_4 and $ZnCl_2$/mp-C_3N_4 materials are presented in Fig. 2. All materials showed type IV isothermal curves with H2 hysteresis loop at $p/p_0 = 0.6$–0.95, indicating that the samples had typical mesoporous structures, along with relatively concentrated pore size distributions. Furthermore, the adsorption curves proceeded further ascent at $p/p_0 > 0.95$, suggesting that these materials contained

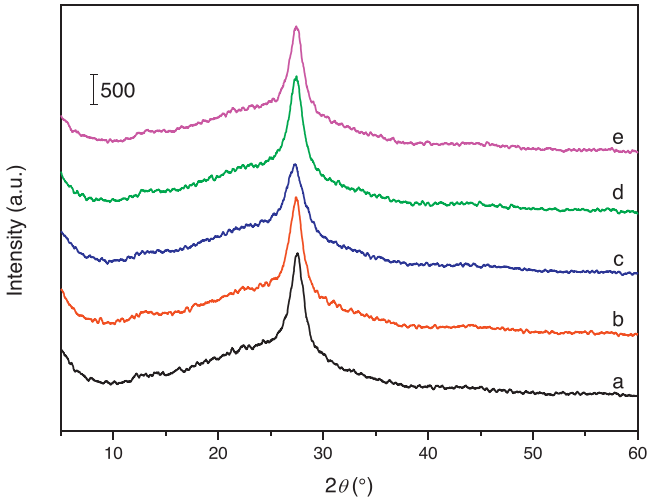

Fig. 1. XRD patterns of mp-C_3N_4 and $m$$ZnCl_2$/mp-$C_3N_4$ materials (a: mp-C_3N_4, b–e: m = 2.5–10 wt%).

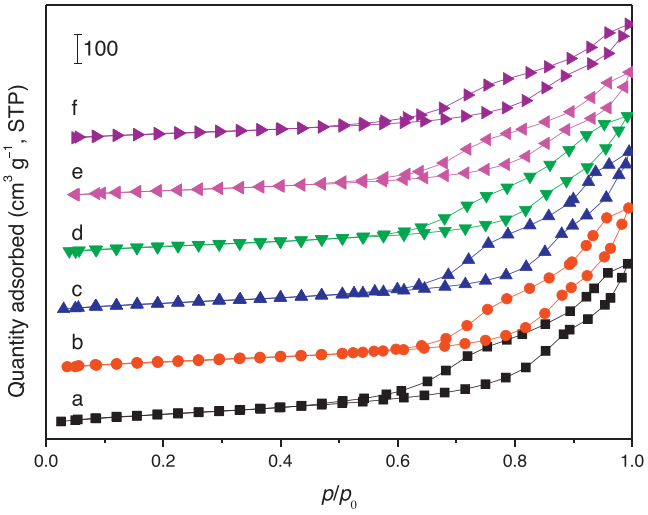

Fig. 2. N_2 adsorption–desorption isotherms of mp-C_3N_4 and $m$$ZnCl_2$/mp-$C_3N_4$ materials (a: mp-C_3N_4, b–f: m = 2.5–12.5 wt%).

Table 1
Textual parameters of mp-C_3N_4 and $ZnCl_2$/mp-C_3N_4 materials.

Sample	S_{BET} ($m^2\ g^{-1}$)	Pore size (nm)	Pore volume ($cm^3\ g^{-1}$)
mp-C_3N_4	298	15.3	0.93
2.5$ZnCl_2$/mp-C_3N_4	244	15.2	0.95
5.0$ZnCl_2$/mp-C_3N_4	232	15.0	0.93
7.5$ZnCl_2$/mp-C_3N_4	231	14.5	0.80
10$ZnCl_2$/mp-C_3N_4	206	12.6	0.72
12.5$ZnCl_2$/mp-C_3N_4	198	10.7	0.67

a small proportion of macropores which should originate from interparticle void. Compared with the pure mp-C_3N_4 sample, the $ZnCl_2$-loaded mp-C_3N_4 materials displayed no apparent change in terms of isotherms, only lower adsorbed quantity. Correspondingly, as listed in Table 1, upon increasing the loading amounts, the textual parameter including surfaces and pore volumes decreased monotonously. However, the pore sizes underwent no obvious decline. This confirmed that after the loading of $ZnCl_2$, the mesostructures of mp-C_3N_4 have well remained.

The information of chemical bonding was investigated by FT-IR technique. As shown in Fig. 3A, the FT-IR spectra of both mp-C_3N_4 and $ZnCl_2$/mp-C_3N_4 exhibited very similar bands. The broad bands located at 3450–3250 cm^{-1} were indicative of primary (i.e. terminal $-NH_2$ groups linked to the edges of graphitic CN sheets) and secondary amines, and physically adsorbed water (H—O—H) molecules [38]. The multiple bands in the range of 1600–1200 cm^{-1} were assigned to the stretching modes of aromatic amines [39]. Furthermore, the sharp transmission peaks with strong intensity at ca. 810 cm^{-1} were evidence of the presence of triazine units [39,40]. Despite these analogies, the spectra of $ZnCl_2$/mp-C_3N_4 materials demonstrated weak bands at ca. 2360 cm^{-1} which have not been detected in that of mp-C_3N_4. The unique bands were attributed to the trapped CO_2 molecules [31]. As mentioned above, owing to the presence of plenty of amine species at the edge of graphitic sheets, mp-C_3N_4 was a typical solid base and could adsorb/absorb ambient acidic CO_2. However, the basic intensity of mp-C_3N_4 was very weak and meanwhile, due to the low detection sensitivity, the adsorbed

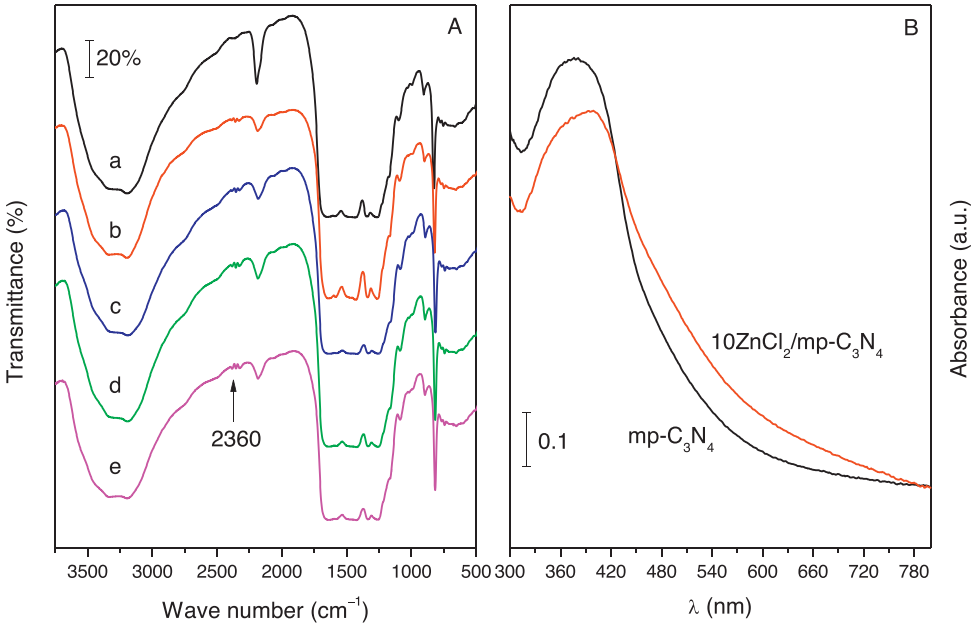

Fig. 3. FT-IR (A) and UV–vis (B) spectra of mp-C_3N_4 and $m$$ZnCl_2$/mp-$C_3N_4$ materials (A: a: mp-C_3N_4, b–e: m = 2.5–10 wt%).

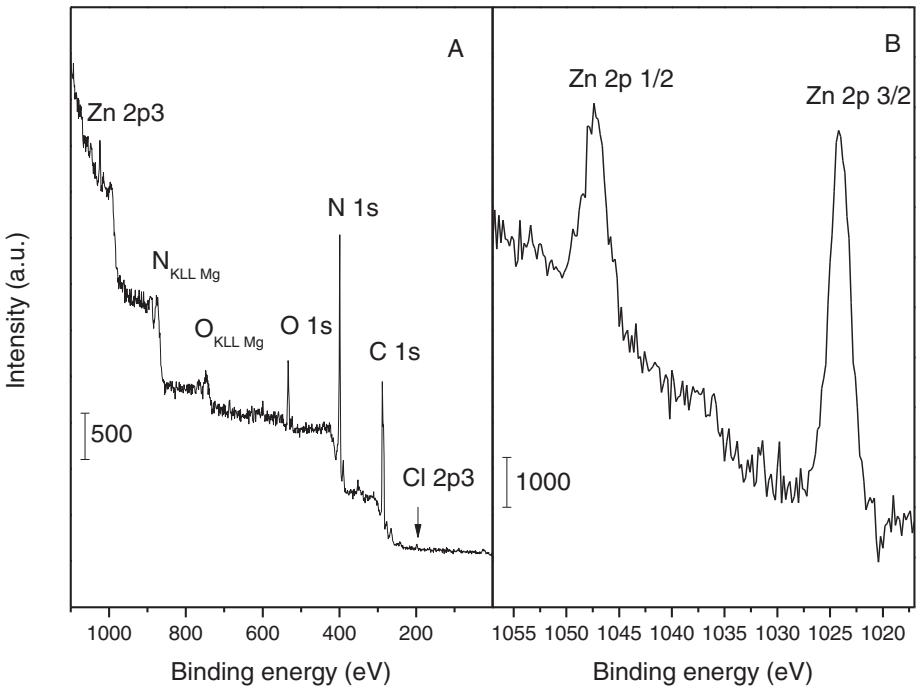

Fig. 4. XPS survey (A) and Zn 2p (B) spectra of $10ZnCl_2/mp\text{-}C_3N_4$.

CO_2 by $g\text{-}C_3N_4$ was hardly detected by the present FT-IR technique. Given this point, it was implied that after the loading of $ZnCl_2$, the total basic intensity of $mp\text{-}C_3N_4$ had been enhanced.

The effect of metal loading on the electronic structure of $mp\text{-}C_3N_4$ was analyzed by UV–vis DRS characterization. As shown in Fig. 3B, the spectrum of $mp\text{-}C_3N_4$ presented a remarkable absorption peak centered at ca. 410 nm, which was derived from bandgap between HOMO and LUMO in the polymeric melon units of $g\text{-}C_3N_4$ [35]. Similarly, in the case of $10ZnCl_2/mp\text{-}C_3N_4$, its spectrum showed a major absorption in UV region. However, the UV absorption edge of $10ZnCl_2/mp\text{-}C_3N_4$ was moved towards longer wavelengths in comparison with that of $mp\text{-}C_3N_4$. The phenomenon has also been previously reported over $g\text{-}C_3N_4$ supported Fe [36], Zn [41], and V [42] catalysts. The shift of absorption peak after the loading of $ZnCl_2$ probably resulted from the d–p repulsion of the Zn 3d and N 2p orbits, namely a host–guest interaction between the $ZnCl_2$ and $g\text{-}C_3N_4$ [36].

XPS technique was further employed to probe the surface chemical environment of the $ZnCl_2/mp\text{-}C_3N_4$ materials and a representative survey spectrum of $10ZnCl_2/mp\text{-}C_3N_4$ was presented in Fig. 4A. The surface of $10ZnCl_2/mp\text{-}C_3N_4$ was mainly constituted of C, N, O, Zn, and Cl species. Wherein, the O element should originate from the adsorbed water due to the mesostructures of $mp\text{-}C_3N_4$. Based on the peak areas calculated, the weight percentage of $ZnCl_2$ was ca. 9.2%, very close to the nominal loading amount of the $10ZnCl_2/mp\text{-}C_3N_4$ sample. The Zn 2p spectrum (Fig. 4B) showed two independent peaks located at 1023 and 1046 eV, corresponding to the signals of Zn 2p 3/2 and 1/2, respectively. The values verified that the chemical valence of Zn element was +2, similar to the results involving $ZnCl_2$ catalysts supported on other materials [43,44].

3.2. Catalyst activity

The $ZnCl_2/mp\text{-}C_3N_4$ materials were employed as solid catalysts for cycloaddition of CO_2 with PO. As listed in Table 2, the catalytic activity acquired over the bare $mp\text{-}C_3N_4$ sample was limited; only a conversion of 10% was received. After the introduction of a small amount of $ZnCl_2$, the catalytic conversion of PO was improved. In the case of the product distribution, the selectivity to the desired PC was over 99%. Further elevating the loading amounts, the activity increased progressively. The highest PO conversion was achieved over the $10ZnCl_2/mp\text{-}C_3N_4$ catalyst, affording a maximum PC yield as much as 72.6%. On the other hand, under the same reaction conditions, the unload $ZnCl_2$ sample exhibited an outstanding PO conversion. It is well documented that zinc halides can efficiently promote the cycloaddition of CO_2 with epoxides to cyclic carbonates [1,10,45]. Compared with homogeneous catalysts, almost all heterogeneous catalysts suffer from lower reaction rates due to mass transfer and diffusion of the reactants to the catalytically active sites. Therefore, it is reasonable that the catalytic activity

Table 2
Catalytic performances of different $ZnCl_2/mp\text{-}C_3N_4$ catalysts[a].

Catalyst	Conv. (%)	Sel. (%)	Yield (%)
$mp\text{-}C_3N_4$	10.4	99.7	10.4
$2.5ZnCl_2/mp\text{-}C_3N_4$	27.9	99.8	27.8
$5.0ZnCl_2/mp\text{-}C_3N_4$	43.6	99.4	43.3
$7.5ZnCl_2/mp\text{-}C_3N_4$	58.2	99.6	58.0
$10ZnCl_2/mp\text{-}C_3N_4$	73.0	99.4	72.6
$12.5ZnCl_2/mp\text{-}C_3N_4$	71.5	99.7	71.3
$ZnCl_2$	97.3	99.5	96.8

[a] Reaction conditions: V_{PO} = 7 mL, V_{DMF} = 3 mL, pCO_2 = 2.5 MPa, T = 140 °C, t = 6 h, and $W_{catal.}$ = 0.2 g.

Table 3
Catalytic performances of cycloaddition reactions of CO_2 under various DMF volumes[a].

Entry	V_{PO} (mL)	V_{DMF} (mL)	Conv. (%)	Sel. (%)	Yield (%)
1	10	0	25.2	99.1	25.0
2	8	2	55.2	99.6	55.0
3	7	3	73.0	99.4	72.6
4	6	4	72.9	99.6	72.6
5	5	5	65.3	99.5	65.0

[a] Evaluated over $10ZnCl_2/mp\text{-}C_3N_4$. Reaction conditions: pCO_2 = 2.5 MPa, T = 140 °C, t = 6 h, and $W_{catal.}$ = 0.2 g.

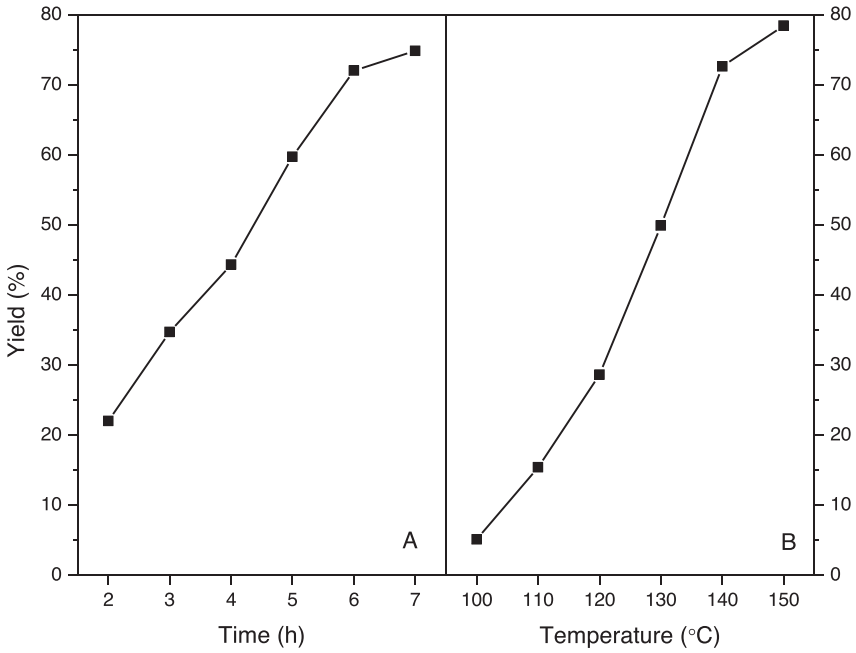

Fig. 5. Effects of reaction time and temperature on the catalytic performances of $10ZnCl_2/mp\text{-}C_3N_4$. Reaction conditions: V_{PO} = 7 mL, V_{DMF} = 3 mL, pCO_2 = 2.5 MPa, and $W_{catal.}$ = 0.2 g.

decreased when $ZnCl_2$ were supported on mp-C_3N_4. However, it should be noted that the reaction catalyzed by $ZnCl_2$ is homogeneous, suffering from difficulty in catalyst separation as well as product purification.

Table 3 shows the catalysts results of cycloaddition reactions of CO_2 catalyzed by the $10ZnCl_2/mp\text{-}C_3N_4$ catalyst with various DMF volumes. Under the DMF-free condition, the PO conversion was 25.2% (entry 1), while after the addition of DMF, the obtained catalytic activity increased noticeably. According to the work reported by Zhong et al., in the CO_2-involving heterogeneous reactions, besides being a solvent, DMF could activate CO_2 molecule by forming carboxylate ion [45]. As expected, with the increase of DMF volume (entries 2–4), the catalytic conversions increased progressively. However, excessive employment of DMF would deteriorate the catalytic activity (entry 5). One possible reason accounting for this phenomenon was that redundant DMF might impede the adsorption of reactants on the surface of the present heterogeneous catalyst, thus undermining the catalytic efficiency. To elucidate the effect of reaction conditions on the catalytic performances, the variations of the catalytic conversions at different reaction time and temperatures were further studied (Fig. 5). At the first 2 h, the catalytic reaction proceeded with a low PO yield of ca. 22% (Fig. 5A). Upon prolonging the evaluation, the catalytic activity increased remarkably but leveled off at 6 h. The reaction temperature was also a key parameter to affect the catalytic performances. As shown in Fig. 5B, the cycloaddition of CO_2 with PO almost hardly reacted under mild temperatures below 110 °C; as the temperature was increased, the PC yield increased drastically. It is widely reported that the cycloaddition reactions of CO_2 with epoxides are typically exothermic processes. Therefore, in viewpoint of its thermodynamic equilibrium, higher temperatures would inhibit the formation of cyclic carbonates [6]. In addition, higher temperatures are liable to result in the polymerization of the cyclic carbonates, and therein deteriorate the catalytic productivity [46]. Considering the above results, a temperature of 140 °C and 6 h were selected as optimal reaction conditions for realizing the highest catalytic activity.

Besides reaction time and temperatures, we also investigated the influence of CO_2 pressure and catalytic amount on the catalytic performances. Under a low pressure of 0.5 MPa (Fig. 6A), the PC yield was *ca.* 40%. As the pressure was elevated, the PC yield increased drastically. However, when the CO_2 pressure was above 2.5 MPa, the productivity showed no significant improvement. Likewise, it has been found that the catalytic performance depended on the catalytic amounts (Fig. 6B). In the absence of any catalyst, the blank test indicated that the PC yield was ca. 5%. After the addition of $10ZnCl_2/mp\text{-}C_3N_4$ catalyst with 0.1 g, the PC yield reached 56.3%. Further increasing the catalytic amount, the PC yield increased progressively while leveled off as the catalyst weight was over 0.2 g.

Table 4
Recycling tests for $10ZnCl_2/mp\text{-}C_3N_4$ in the cycloaddition reactions of CO_2[a].

Catalytic run	Conv. (%)	Sel. (%)
1	73.0	99.4
2	59.3	99.2
3	58.7	99.4
4	57.9	99.5

[a] Reaction conditions: V_{PO} = 7 mL, V_{DMF} = 3 mL, pCO_2 = 2.5 MPa, $W_{catal.}$ = 0.2 g, t = 6 h, and T = 140 °C.

In addition to the catalytic activity, recyclability is also a very important criterion to evaluate a heterogeneous catalyst. Regarding this issue, the spent $10ZnCl_2/mp\text{-}C_3N_4$ catalysts was then rinsed by ethanol for several times, dried overnight, and reused directly for another run. The corresponding catalytic results are listed in Table 4. The PO conversion acquired within the first recycle (i.e. the second run) was ca. 60%, appreciably lower than the value obtained in its first run. In the case of the product distribution, the selectivity to PC was higher than 99%. As mentioned above, mp-C_3N_4 materials were prepared using cyanamide as a precursor. The transformation from cyanamide to the final g-C_3N_4 underwent a series of co-condensation steps, and therefore there existed a large amount of uncondensed *N*-containing fragments [6,47], which thereafter reacted with metal halides after the loading. However, due to the intrinsically unstable disadvantage of the *N*-containing fragments in mp-C_3N_4, a small proportion of such species would inevitably leach out and diffuse into the liquid phase during the reactions, resulting in the noticeable decline in the recycle test. Despite the

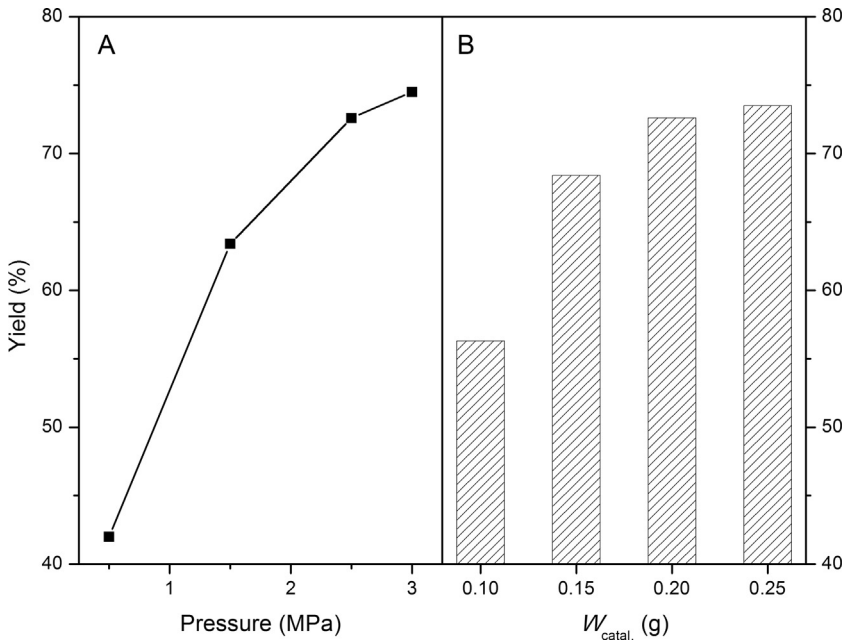

Fig. 6. Influence of CO_2 pressure and catalyst amount on the catalytic performance of $10ZnCl_2/mp\text{-}C_3N_4$. Reaction conditions: V_{PO} = 7 mL, V_{DMF} = 3 mL, t = 6 h, and T = 140 °C.

Table 5
Catalytic performances of various mp-C_3N_4-supporting catalysts[a].

Entry	Catalyst	Conv. (%)	Sel. (%)	Yield (%)
1	$ZnCl_2/mp\text{-}C_3N_4$	73.0	99.6	72.7
2	$ZnBr_2/mp\text{-}C_3N_4$	99.2	99.7	98.9
3	$CoCl_2/mp\text{-}C_3N_4$	70.4	99.6	70.1
4	$FeCl_3/mp\text{-}C_3N_4$	77.2	99.8	77.0
5	$NiCl_2/mp\text{-}C_3N_4$	63.7	99.6	63.4
6	$MgCl_2/mp\text{-}C_3N_4$	71.7	99.5	71.3

[a] The molar amounts of halide compounds were all 0.73 mmol. Reaction conditions: V_{PO} = 7 mL, V_{DMF} = 3 mL, pCO_2 = 2.5 MPa, T = 140 °C, t = 6 h, and $W_{catal.}$ = 0.2 g.

loss of catalytic activity in the first recycle, the following two catalytic tests, demonstrated highly stable PO conversions. This phenomenon evidenced that the $ZnCl_2/mp\text{-}C_3N_4$, subjected with the initial run under high temperature and pressure, would become chemically and physically stable.

As revealed above, the PO conversion obtained over the pristine mp-C_3N_4 material was only 10%; by contrast, the mp-C_3N_4-supported $ZnCl_2$ samples could catalyze the cycloaddition reactions of CO_2 with much higher yields. Undoubtedly, in such catalytic system, mp-C_3N_4 mainly acted as a catalytic support whereas $ZnCl_2$ was the catalytically active compound. In this study, besides $ZnCl_2$, we have also prepared a series of transition metal halide catalysts supported on mp-C_3N_4 and submitted them to cycloaddition reactions of CO_2. It should be noted that the loading amounts of these metal halides were fixed as 0.73 mmol, the same to the $10ZnCl_2/mp\text{-}C_3N_4$ catalyst. As summarized in Table 5, the supported $ZnBr_2$ catalyst (entry 2) displayed superior activity to the supported $ZnCl_2$ one, affording a 99% PC yield. Other supported metal halides, including $CoCl_2$, $FeCl_3$, $NiCl_2$, and $MgCl_2$ (entries 3–6) also exhibited notably high catalytic activity (>60%). Obviously, the supported metal halides play a crucial role in promoting the catalytic cycloaddition.

According to the previously published work [1,29,48,49], a possible reaction mechanism for cycloaddition of CO_2 catalyzed by metal halide supported on mp-C_3N_4 was proposed, (Scheme 1). First, due to its insufficient polycondensation, there existed abundant uncondensed species, in the forms of primary and/or secondary amines, at the edges of graphitic sheets of mp-C_3N_4.

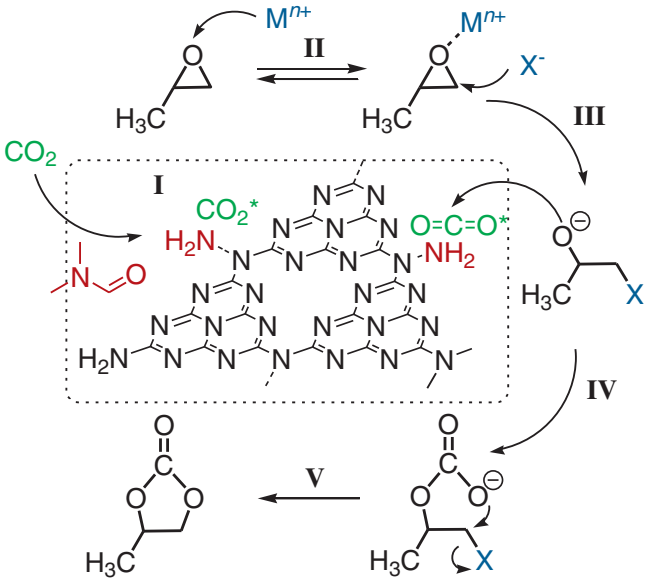

Scheme 1. A possible mechanism of cycloaddition of CO_2 with PO catalyzed by metal halide supported on mp-C_3N_4.

Especially, the high surface area and accessible mesopores enabled mp-C_3N_4 to expose much more defect amines on its surface. With this unique surface environment of mp-C_3N_4, and DMF as a Lewis base [45], CO_2 molecules were adsorbed by the N atoms through an acid–base interaction (step **I**) and transformed into activated CO_2 species. On the other hand, the metal cation coordinated with oxygen atom of PO and led to the polarization of C—O bonds (step **II**). After that, the halogen anion attacked a carbon atom of PO, resulting in a ring opening and generating a haloalkoxy anion (step **III**). The subsequent haloalkoxy anion attacked the activated CO_2 molecule located on the surface of mp-C_3N_4 and generated a linear halocarbonate (step **IV**). Subsequently, the halocarbonate transformed into PC via a ring closing (step **V**), and meanwhile yielded the halogen anion. In this sense, it is reasonable to explain the higher catalytic activity obtained in entry 2 of Table 5 than that of entry 1, as the

leaving ability of Br^- was higher than Cl^-, thereby much more easily actuating the ring-closing reaction [50].

4. Conclusion

In summary, mesoporous g-C_3N_4 was employed as a catalytic support to load $ZnCl_2$. The synthesized $ZnCl_2$/mp-C_3N_4 demonstrated superior catalytic activity to the bare mp-C_3N_4 in the cycloaddition of PO to PC. The highest PC yield was 72.6% obtained over 10$ZnCl_2$/mp-C_3N_4. In addition, other metal halide catalysts supported on mp-C_3N_4 exhibited high PO conversion (>63%). In the proposed mechanism, mp-C_3N_4 having high surface area and mesostructures mainly served as a solid base to adsorb CO_2 while metal halide was a key formulation to activate PO molecule via polarizing O atom and opening its ring by metal cation and halide anion, respectively. Although the catalytic activities received over the supported metal halide catalysts were lower than those obtained over the pure ones, the utilization of mp-C_3N_4 solid enabled metal halides to be heterogeneous catalysts, thus rendering convenience in catalyst–product separation. It is anticipated that mp-C_3N_4 would be widely applied in heterogeneous organocatalysis involving CO_2 conversion.

Acknowledgments

This work was supported by National Natural Science Foundation of China (21203014), Jiangsu Key Laboratory of Advanced Catalytic Materials and Technology (BM2012110), and the Project Funded by the Priority Academic Program Development of Jiangsu Higher Education Institutions.

References

[1] S.-S. Wu, X.-W. Zhang, W.-L. Dai, S.-F. Yin, W.-S. Li, Y.-Q. Ren, C.-T. Au, Appl. Catal. A 341 (2008) 106–111.
[2] C.-X. Miao, J.-Q. Wang, Y. Wu, Y. Du, L.-N. He, ChemSusChem 1 (2008) 236–241.
[3] M. North, R. Pasquale, C. Young, Green Chem. 12 (2010) 1514–1539.
[4] K.M.K. Yu, I. Curcic, J. Gabriel, S.C.E. Tsang, ChemSusChem 1 (2008) 893–899.
[5] W.-L. Dai, B. Jin, S.-L. Luo, S.-F. Yin, X.-B. Luo, C.-T. Au, J. CO_2 Util. 3–4 (2013) 7–13.
[6] J. Xu, F. Wu, Q. Jiang, Y.-X. Li, Catal. Sci. Technol. 5 (2015) 447–454.
[7] X.-B. Lu, Y.-J. Zhang, B. Liang, X. Li, H. Wang, J. Mol. Catal. A 210 (2004) 31–34.
[8] R. Srivastava, D. Srinivas, P. Ratnasamy, J. Catal. 233 (2005) 1–15.
[9] J.-Q. Wang, J. Sun, W.-G. Cheng, C.-Y. Shi, K. Dong, X.-P. Zhang, S.-J. Zhang, Catal. Sci. Technol. 2 (2012) 600–605.
[10] J. Sun, L. Wang, S. Zhang, Z. Li, X. Zhang, W. Dai, R. Mori, J. Mol. Catal. A 256 (2006) 295–300.
[11] W.-L. Dai, S.-L. Luo, S.-F. Yin, C.-T. Au, Appl. Catal. A 366 (2009) 2–12.
[12] L.-F. Xiao, F.-W. Li, J.-J. Peng, C.-G. Xia, J. Mol. Catal. A 253 (2006) 265–269.
[13] X. Zhang, D. Wang, N. Zhao, A.S. Al-Arifi, T. Aouak, Z.A. Al-Othman, W. Wei, Y. Sun, Catal. Commun. 11 (2009) 43–46.
[14] W.-L. Dai, L. Chen, S.-F. Yin, S.-L. Luo, C.-T. Au, Catal. Lett. 135 (2010) 295–304.
[15] B.M. Bhanage, S.-I. Fujita, Y. He, Y. Ikushima, M. Shirai, K. Torii, M. Arai, Catal. Lett. 83 (2002) 137–141.
[16] B.M. Bhanage, S. Fujita, Y. Ikushima, K. Torii, M. Arai, Green Chem. 5 (2002) 71–75.
[17] K. Yamaguchi, K. Ebitani, T. Yoshida, H. Yoshida, K. Kaneda, J. Am. Chem. Soc. 121 (1999) 4526–4527.
[18] W.-L. Dai, S.-F. Yin, R. Guo, S.-L. Luo, X. Du, C.-T. Au, Catal. Lett. 136 (2010) 35–44.
[19] J. Zhu, P. Xiao, H. Li, S.A.C. Carabineiro, ACS Appl. Mater. Inter. 6 (2014) 16449–16465.
[20] F. Su, S.C. Mathew, L. Möhlmann, M. Antonietti, X. Wang, S. Blechert, Angew. Chem. Int. Ed. 50 (2011) 657–660.
[21] P. Zhang, Y. Gong, H. Li, Z. Chen, Y. Wang, Nature Commun. 4 (2013) 1593.
[22] Y. Zheng, J. Liu, J. Liang, M. Jaroniec, S.Z. Qiao, Energy Environ. Sci. 5 (2012) 6717–6731.
[23] M. Kim, S. Hwang, J.-S. Yu, J. Mater. Chem. 17 (2007) 1656–1659.
[24] S.S. Park, S.-W. Chu, C. Xue, D. Zhao, C.-S. Ha, J. Mater. Chem. 21 (2011) 10801–10807.
[25] F. Goettmann, A. Fischer, M. Antonietti, A. Thomas, Angew. Chem. Int. Ed. 45 (2006) 4467–4471.
[26] X. Jin, V.V. Balasubramanian, S.T. Selvan, D.P. Sawant, M.A. Chari, G.Q. Lu, A. Vinu, Angew. Chem. Int. Ed. 48 (2009) 7884–7887.
[27] Z. Long, Y. Zhou, G. Chen, W. Ge, J. Wang, Sci. Rep. 4 (2014) 3651.
[28] Y. Wang, J. Yao, H. Li, D. Su, M. Antonietti, J. Am. Chem. Soc. 133 (2011) 2362–2365.
[29] Q. Su, J. Sun, J. Wang, Z. Yang, W. Cheng, S. Zhang, Catal. Sci. Technol. 4 (2014) 1136–1138.
[30] M.B. Ansari, B.-H. Min, Y.-H. Mo, S.-E. Park, Green Chem. 13 (2011) 1416–1421.
[31] M.B. Ansari, H. Jin, S.-E. Park, Catal. Sci. Technol. 3 (2013) 1261–1266.
[32] Z. Huang, F. Li, B. Chen, T. Lu, Y. Yuan, G. Yuan, Appl. Catal. B 136 (2013) 269–277.
[33] F. Su, M. Antonietti, X. Wang, Catal. Sci. Technol. 2 (2012) 1005–1009.
[34] J. Xu, T. Chen, Q. Jiang, Y.-X. Li, Chem. -Asian J. 9 (2014) 3269–3277.
[35] J. Zhu, Y. Wei, W. Chen, Z. Zhao, A. Thomas, Chem. Commun. 46 (2010) 6867–6965.
[36] X. Wang, X. Chen, A. Thomas, X. Fu, M. Antonietti, Adv. Mater. 21 (2009) 1609–1612.
[37] A. Thomas, A. Fischer, F. Goettmann, M. Antonietti, J.-O. Müller, R. Schlögl, J.M. Carlsson, J. Mater. Chem. 18 (2008) 4893–4908.
[38] J. Xu, H.-T. Wu, X. Wang, B. Xue, Y.-X. Li, Y. Cao, Phys. Chem. Chem. Phys. 15 (2013) 4510–4517.
[39] M.J. Bojdys, J.-O. Müller, M. Antonietti, A. Thomas, Chem. -Eur. J. 14 (2008) 8177–8182.
[40] J. Liu, T. Zhang, Z. Wang, G. Dawson, W. Chen, J. Mater. Chem. 21 (2011) 14398–14401.
[41] B. Yue, Q. Li, H. Iwai, T. Kako, J. Ye, Sci. Technol. Adv. Mater. 12 (2011) 034401.
[42] J. Xu, Q. Jiang, T. Chen, F. Wu, Y.-X. Li, Catal. Sci. Technol. 5 (2015) 1504–1513.
[43] S.A. Schmidt, N. Kumar, A. Shchukarev, K. Eränen, J.-P. Mikkola, D.Y. Murzin, T. Salmi, Appl. Catal. A 468 (2013) 120–134.
[44] S.K. Pillai, S. Hamoudi, K. Belkacemi, Appl. Catal. A 455 (2013) 155–163.
[45] S. Zhong, L. Liang, B. Liu, J. Sun, J. CO_2 Util. 6 (2014) 75–79.
[46] L. Han, H. Li, S.-J. Choi, M.-S. Park, S.-M. Lee, Y.-J. Kim, D.-W. Park, Appl. Catal. A 429 (2012) 67–72.
[47] K.K. Han, C.C. Wang, Y.Y. Li, M.M. Wan, Y. Wang, J.H. Zhu, RSC Adv. 3 (2013) 9465–9469.
[48] J. Sun, W. Cheng, Z. Yang, J. Wang, T. Xu, J. Xin, S. Zhang, Green Chem. 16 (2014) 3071–3078.
[49] J. Sun, J. Wang, W. Cheng, J. Zhang, X. Li, S. Zhang, Y. She, Green Chem. 14 (2012) 654–660.
[50] Y. Zhou, S. Hu, X. Ma, S. Liang, T. Jiang, B. Han, J. Mol. Catal. A 284 (2008) 52–57.